Frequency Tunable Filtenna Using Defected Ground Structure Filter in the Sub-6 GHz for Cognitive Radio Applications

Progress In Electromagnetics Research C, Vol. 118, 213–229, 2022

Frequency Tunable Filtenna Using Defected Ground Structure Filter in the Sub-6 GHz for Cognitive Radio Applications

Aicha Bembarka[1, *], Larbi Setti[1], Abdelwahed Tribak[2], Hamza Nachouane[3], and Hafid Tizyi[2]

Abstract—In this paper, a new frequency tunable filtering-antenna (so-called filtenna) is inspired by a Defected Ground Structure (DGS) band-pass filter for the fifth generation picocell base stations. It is intended for use in Cognitive Radio (CR) communications within the European Union Sub-6 GHz spectrum, which ranges between 3.4 and 3.8 GHz. Firstly, a Wideband (WB) monopole antenna is proposed where the operational frequencies cover 3.15–4.19 GHz, taking the 10-dB return loss level as a threshold. A band-pass filter of a Semi-Square Semi-Circle shape is integrated into the WB antenna ground to obtain the communicating filtenna. The narrowband frequency tunability is achieved by changing two varactor diode capacitances located in the filter slots. The antenna is prototyped occupying a total space of $60 \times 80 \times 0.77\,\text{mm}^3$, then tested to verify the simulated results. Three operating frequencies 3.4, 3.6, and 3.8 GHz of the filtenna are studied in terms of return loss, realized gain, and radiation patterns which verify that the frequency shift has almost no effect on the antenna performance. The filtenna has a maximum gain of 4.5 dBi in measurements and 3.47 dBi in simulations. The obtained results have proved their efficiency for CR communications.

1. INTRODUCTION

In the past decades, wired network was the most serviceable technology used in communication services. Nowadays, employing remote networks (i.e., communications without using cables) which are known by the name of "wireless networks" in the transmission of data or information becomes an integral part of several types of communicating devices. Data in this new technology can be transmitted and received without any conductor through Radio Frequency (RF) signals. This development came as a result of several reasons, and among them we found that many business operators are chasing after maximizing their funding while guaranteeing reliable, low cost, and more secure data transmission. On the other hand, in March 2011 the cost of copper wire swiftly increased to nearly 5$ per pound, whereas it was under 1$ per pound in 2001 [1]. Moreover, on February 25th, 2018, Vodafone and Samsung joined hands by making a partnership in a "V-smart by Vodafone" services. These services are based on smart connected devices such as Wi-Fi hubs, Sirens, Security Cameras, and Vodafone "V-Home Alarm Assistant" [2].

According to the Qualcomm report made in April 2020, in more than 115 countries around the world, more than 340 operators were investigating 5G. The implementation of 5G systems can happen either in the mid-band also called "Sub-6 GHz band" or in the millimeter-waves (mm-waves) region [3]. The Federal Communication Commission (FCC) has defined the usable frequencies for the 5G spectrum

Received 14 January 2022, Accepted 21 February 2022, Scheduled 27 February 2022
* Corresponding author: Aicha Bembarka (aichabembarka@gmail.com).
[1] Laboratory of Sciences and Advanced Technologies (LSTA), Polydisciplinary Faculty of Larache (FPL), Abdelmalek Essaadi University, Tetouan, Morocco. [2] Department of Electronics Microwaves and Optics, National Institute of Posts and Telecommunications (INPT), Rabat, Morocco. [3] Department of Microtechnology and Nanoscience, Chalmers University of Technology, Gothenburg, Sweden.

in Europe on the Sub-6 GHz within the range of 3.4–3.8 GHz, and for millimeter frequencies it is above 24 GHz. At the mm-waves, the frequencies are higher, so the wavelengths get shorter, which results in a short propagation distance, leading to a high data rate and making it possible to reduce the size of systems or components. But in return, the power losses in the mm-RF frequencies arise according to the medium used in propagation. Rain and fog are the major factors of the atmospheric propagation losses, and they increase rapidly with frequency as demonstrated in Figure 1 of Reference [4]. It can be clearly seen that the rain attenuation is the highest, given by the discrete line. We can add to these two absorbers of the mm-waves the effect of attenuation coming from hail, snow, and losses due to oxygen and water vapor. Consequently, researchers and scientists focused on studying the 5G technology in lower frequencies [4].

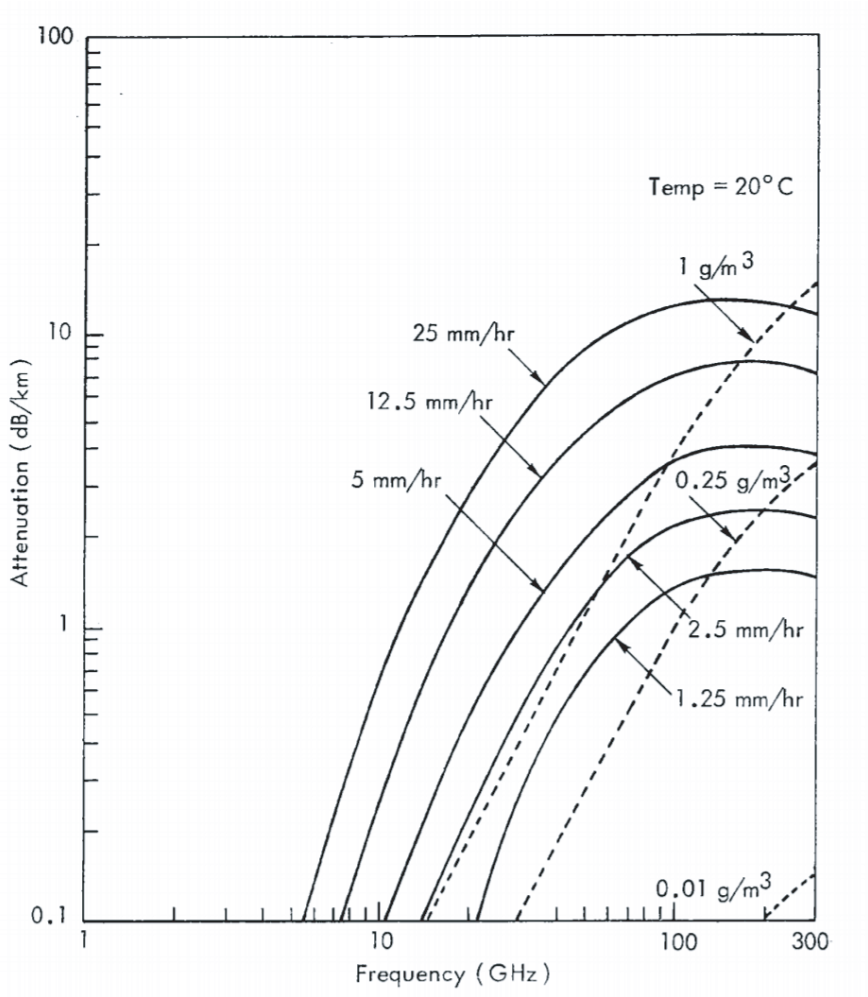

Figure 1. Effect of rain and fog on the frequency [4].

The demand of users for wireless technologies increases day by day causing a huge compression in the predefined limited spectrum. Additionally, sometimes RF signals are strongly exposed to fading and path losses, thus it is very difficult for outdoor signals to reach out well to indoor devices in very dense areas. Picocell base stations and CRs are two options that help to overcome these issues, besides making use of the same frequency at the same cell, they make the speed of the transceived data faster by shortening the communication distance. CRs detect automatically and rapidly the strength of the received signals and the unused spectrum by the licensed user (white space). These white holes could be accessible without making interferences with the licensed user by looking at the strength of the signal [5].

The transmit/receive tasks in both picocell base stations and CRs need components with high performances with low complexity (i.e., fabricated with the minimum number of lumped elements, which leads to decreasing the cost and power consumption), and are suitable for planar circuits. So, in order to ensure getting stable communication at a specific frequency in CRs, bandpass filters have been proposed. However, designing the antenna and filter individually can lead to larger space and increase the cost of realization which is not recommended. Therefore, for space minimization, the concept of integrating both the antenna and filter in a single structure appears as a potential solution, and it is known as filter-antenna or filtenna. In the literature, several approaches containing filtennas have been discussed [6–8]. Some authors suggested more than one CR antenna designed separately at the same substrate, an antenna for communication and another for sensing [9–11]. Nevertheless, the mutual coupling reduction between the two antennas should be taken into consideration to avoid any degradation of the antenna performance. Although the CR consists of a wideband antenna and a narrowband antenna, the wideband antenna presents an inherent gain-bandwidth product limitation, and it gives a low signal-to-noise ratio in the spectrum sensing [12]. As a solution to all the previously mentioned issues in the CR environments, narrowband frequency tunable filtennas have appeared for communication tasks and have been proposed in many pieces of literature [12, 13]. For example, two different configurations of band-pass filters were implemented to the same antenna in [13] to ensure the communication tasks in CR environments. A T-shaped band-pass filter helped to tune the antenna characteristics between 4.26 and 5.94 GHz, while an H-shaped filter altered the resonant frequency range from 3.85 to 5.58 GHz. Regardless of their high performance, these two antennas operate on frequencies other than the Sub-6 GHz band. On the other hand, tunable antennas covering the Sub-6 GHz spectrum have appeared in the literature [14–16]. In [14], an antenna of 1.7 dBi gain has been presented. A single-pole 4-throw switch was used to tune its resonant frequency between 2.5 and 3.6 GHz; however, the switch and the antenna were on distinct substrates, resulting in a wide area of $60 \times 100 \times 1\,\text{mm}^3$. Unless the antenna and tuning components in [15, 16] share the same substrate and the maximum gain in [16] is acceptable at 3 dBi, their sizes are large of $136 \times 68 \times 6\,\text{mm}^3$ and $80 \times 80 \times 2.4\,\text{mm}^3$, respectively. Hence, the majority of antennas in the literature have either a large dimension or a poor gain, or both, or work outside the Sub-6 GHz band.

In this paper, a compact monopole antenna with frequency tunability has been proposed. Herein, the fundamental idea is to achieve an uncomplicated structure for CR communications at a lower cost. The proposed antenna operates in the Sub-6 GHz band and maintains good gain while being small in size. It has a maximum gain of 4.5 dBi and an overall dimension of $60 \times 80 \times 0.77\,\text{mm}^3$. The filter-antenna is designed by using a band-pass filter in a WB antenna ground plane. By integrating varactor diodes in the filter slots and controlling the reverse voltage applied to them through the biasing network, the operating frequency shift has been obtained. Hence, both filtering and radiation were performed using a single configuration. All simulations and their optimizations are performed using CST microwave Studio which is based on the FIT method and then verified using the FEM method of HFSS. The proposed WB antenna design process simulated realized gain, and a discussion of where to integrate the Semi-Square Semi-Circle bandpass filter are presented in Section 2. Also, the simulated and measured results of return loss are compared. The band-pass filter is constructed from a band-stop filter whose configuration and results are illustrated in Section 3. In Section 4, the proposed tunable filtenna for picocell CR applications is presented, and its simulated and measured results are discussed. The paper's conclusion is drawn in Section 5.

2. WIDEBAND ANTENNA DESIGN AND ANALYSIS

A WB antenna of a monopole type is illustrated in Figure 2. A low-cost Rogers RO4725JXR substrate is selected to construct the proposed antenna, having 0.77 mm in thickness, a dielectric permittivity of 2.55, and a loss tangent of 0.0026. This structure is fed through a 50 Ω CPW line of 3 mm in width and 31.9 mm in length. A trapezoidal-shaped ground plane is designed symmetrically to the feed line, which showed its effectiveness in improving the antenna performance, as demonstrated below. The radiating element is composed of two rectangular patches linked via a transmission line that has the same width as the feed line and a length of 5.6 mm and helps to accomplish the wide impedance bandwidth. The geometry of the basic WB antenna is presented in Figure 1 which occupies a space of $60 \times 80 \times 0.77\,\text{mm}^3$.

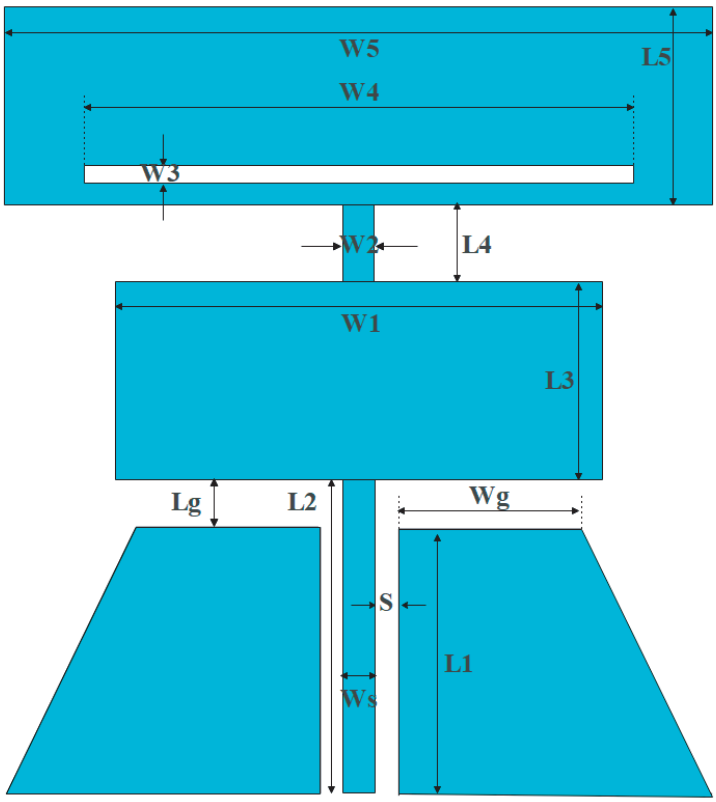

Figure 2. The geometry of the proposed WB antenna.

The antenna was fabricated with the help of the LPKF machine and tested using Anritsu MS2028C VNA, which are available within the INPT Laboratory. The final design parameters are summarized as follows (units in mm): $W_S = 3$, $S = 0.7$, $W_g = 17.13$, $W_1 = 39.47$, $W_2 = 3$, $W_3 = 1.5$, $W_4 = 51.43$, $W_5 = 60$, $L_g = 1.9$, $L_1 = 30$, $L_2 = 31.9$, $L_3 = 22.5$, $L_4 = 5.6$, $L_5 = 20$.

2.1. Design Process

The purpose of this paper is to realize a frequency tunable antenna that covers frequencies between 3.4 and 3.8 GHz (the Sub-6 GHz band). For that reason and from a first basic WB antenna, we will construct the tunable monopole antenna. The basic antenna was built through various steps, which are summarized in Figure 3. At first, we designed the monopole antenna that has a rectangular ground plane and a radiated element formed by two different patches linked directly to each other presented by Antenna_1, but this ground shape did not fulfill the requirements needed for antennas. Thus, changing the ground plane shape to trapezoid rather than rectangle helped the antenna to resonate from 3.42 to 3.95 GHz for a −10 dB return loss level as shown in Figure 3 (Antenna_2). However, this band remains small, and the matching is weak. That can be explained by the fact that a very little amount of current reaches the upper radiator patch. For that reason, to expand the bandwidth of Antenna_2 we narrowed the space linking the two patches and also etched a slot into the upper patch, and its corresponding reflection coefficient is illustrated in Figure 4 of Antenna_3. The narrowed space helped to concentrate more currents toward the upper patch, while the slot contributed to the current deviation for greater radiation and broader bandwidth. Therefore, a wide impedance bandwidth and good matching are obtained using Antenna_3 as a final structure, operating in the frequency range 3.13–4.04 GHz with the minimum reflection coefficient of −26 dB at 3.7 GHz. By increasing the basic antenna bandwidth, our tunable filtenna not only can work in the Sub-6 GHz band but also can function in the WiMax (3–3.4 GHz) and C-band (3.8–4.2 GHz). In this paper, our main band is the Sub-6 GHz, then to avoid the cost of measurement we will focus only on this band.

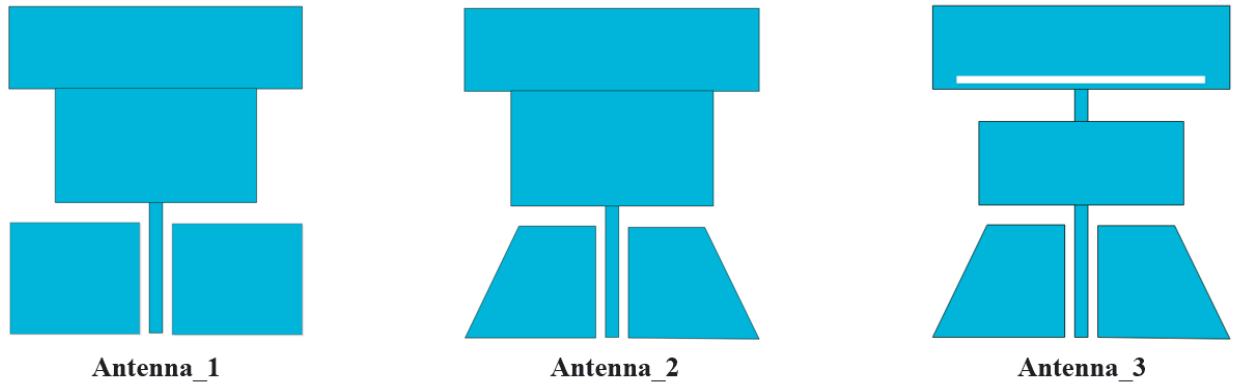

Figure 3. Evolution of the wideband antenna, rectangular ground plane (Antenna_1); trapezoidal ground plane (Antenna_2); proposed wideband antenna (Antenna_3).

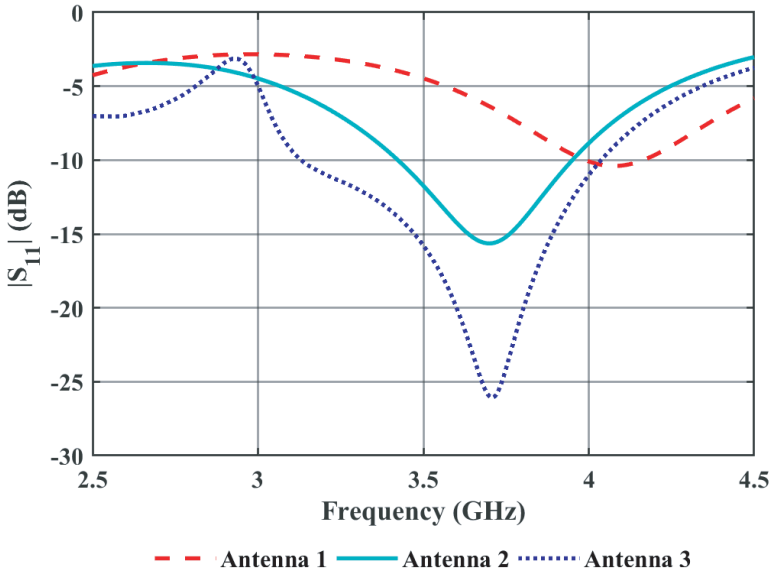

Figure 4. Simulated return loss of the WB antenna evolution.

2.2. Parametric Study

Aiming to study the effect of the basic antenna parameters on the bandwidth and impedance matching, the study includes two parameters L_g and W_2. The distance between the ground plane and the lower patch (L_g) is investigated in Figure 5. It can be clearly noticed from this figure that as this distance increases the antenna shows a better impedance matching, and the resonant frequencies shift toward the left, which means that the distance L_g is inversely proportional to the frequency. The value of this parameter is selected to be 1.9 mm since this value covered the Sub-6 GHz band and showed a good impedance matching and at the same time showed a larger impedance bandwidth than L_g of 2.6 mm.

For different values of W_2, the results of the simulated return loss are shown in Figure 6. Although the return loss attains 30 dB when W_2 is equal to 5 mm, the bandwidth is smaller than the W_2 value of 1 and 3 mm, and 14 mm gives the worst results among those values. Therefore, to obtain a wide bandwidth along with a good impedance matching W_2 is set to 3 mm.

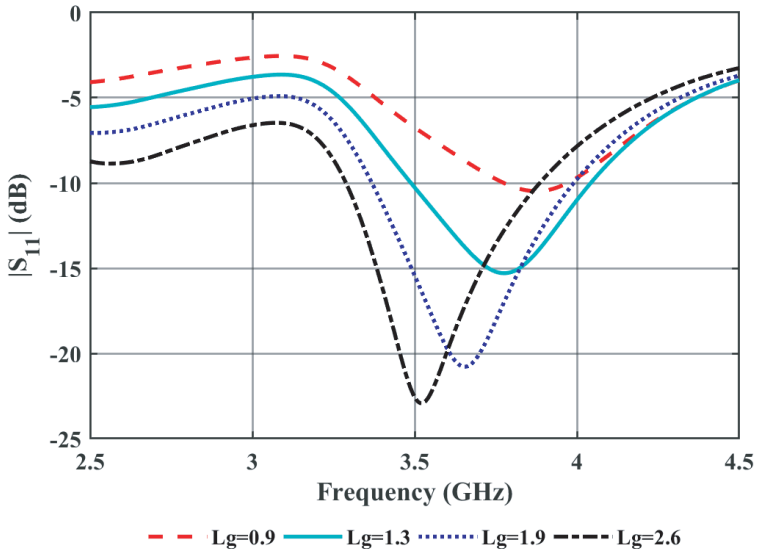

Figure 5. Simulated return loss versus parameter L_g in mm unit.

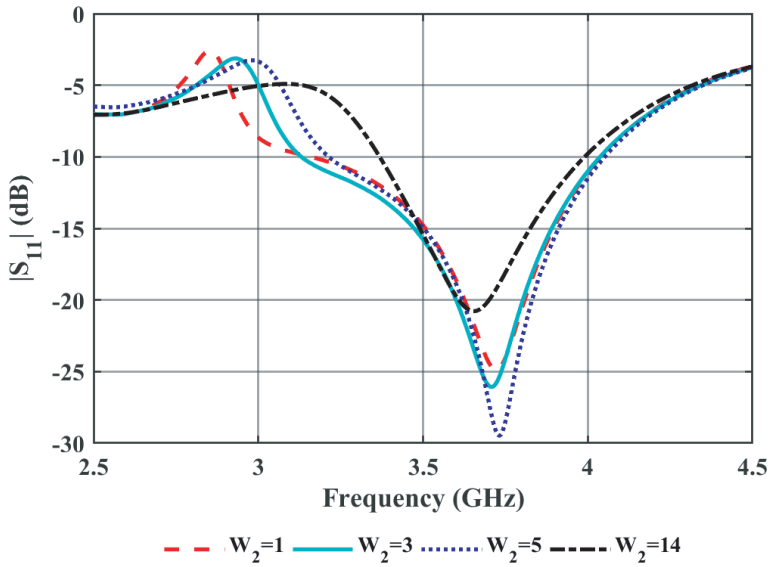

Figure 6. Simulated return loss versus parameter W_2 in mm unit.

2.3. Simulated and Measured Results of the Wideband Antenna

As aforementioned, manufacturing has been done using the LPKF machine. A comparison between the simulated and measured results of the reflection coefficient and a photograph of the first antenna are shown in Figure 7. It can be seen from this figure that for an S_{11} below 10 dB the simulated bandwidth is 3.13–4.04 GHz (25.38%) and 3–3.94 GHz which is approximate 908 MHz and 940 MHz (27%) using CST and HFSS, respectively. As is evident from the graph of measurements, the antenna has an impedance bandwidth between 3.15 and 4.19 GHz (28.33%), which is approximately 3% larger than the simulated results. The simulated and experimented results are in good concordances, and the slight shifts of the return loss toward left from HFSS or the difference observed in the measurements at the lower frequencies could be attributed to several reasons such as the homogeneity of the substrate material, manufacturing, and soldering [17] or due to test errors.

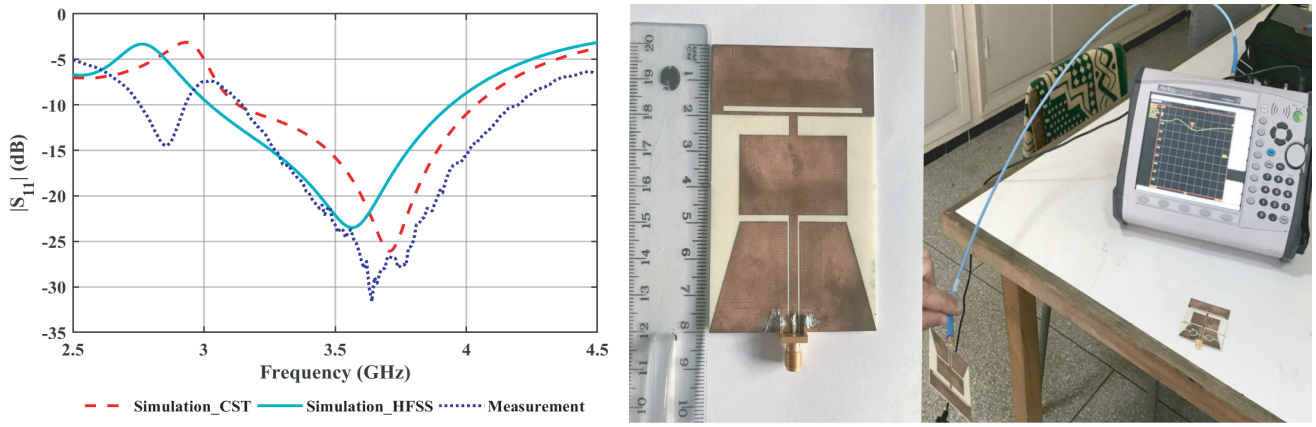

(a) (b)

Figure 7. (a) Simulated and measured return loss and (b) photograph of fabrication/measurement, of the proposed wideband antenna.

2.4. Gain and Current Distribution of the Wideband Antenna

Antenna gain is fundamental to evaluating its performance, and having a sufficient gain allows the transmitted signal to reach its destination easily. The gain of the proposed WB antenna versus frequency is presented in Figure 8(a). From this figure, the antenna gain can reach 4.82 dBi using CST and 4.08 dBi in HFSS. Therefore, the proposed basic antenna showed its effectiveness and at the same time covered a wideband spectrum from 3.15 GHz to 4.19 GHz, which includes the targetable Sub-6 GHz band. In the next sections, a DGS passing band filter will be etched on the WB antenna to realize the tunable filter-antenna. In order to define the suitable place in which to put the filter, Figure 8(b) shows the obtained surface current distribution of the proposed antenna from CST at 3.6 GHz. It can be seen from this figure that a large surface current density is located in slots between the feed line and the ground plane, also at the lower edge of the lower patch, and a small amount is seen at ground plane edges. The region that has a high current density is the best place for the filter and acts as a transmitting region.

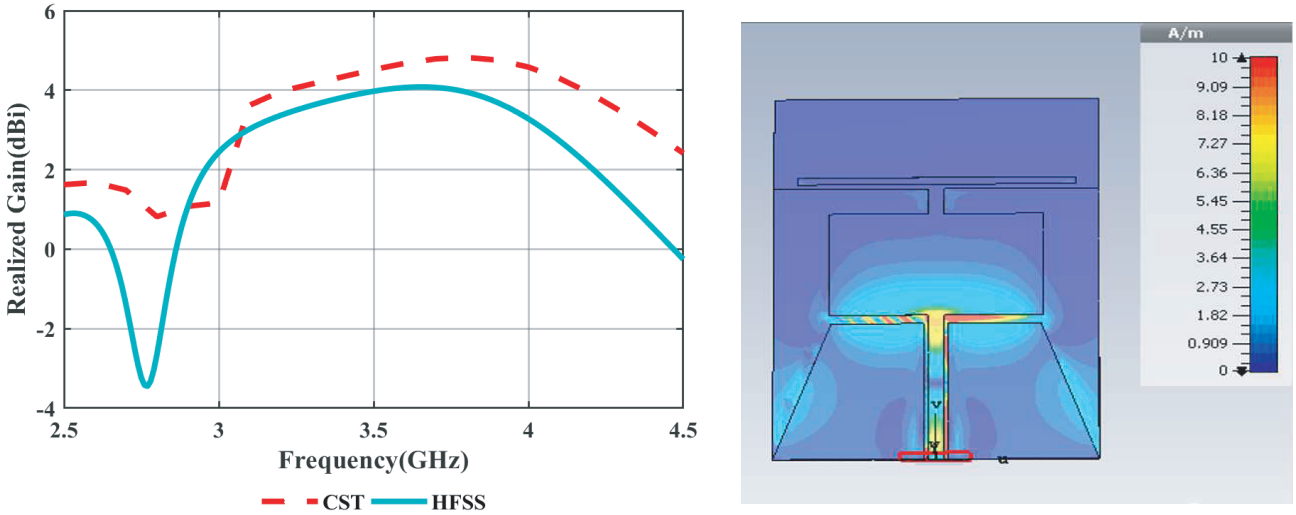

(a) (b)

Figure 8. (a) Simulated realized gain and (b) current distribution at 3.6 GHz, of the WB antenna.

3. DESIGN OF THE BAND-PASS FILTER CONFIGURATION

A bandpass filter is a microwave component that allows signals between two specific frequencies to pass through it, but in return, it attenuates signals at other frequencies. The band-pass could be of a wideband type or a narrow band according to the filter used. From the most frequently used configurations of planar bandpass filters, we can find parallel-coupled [18], square patch resonators [19], inter-digital coupled lines [20], quarter-wavelength resonators [21], and hairpin lines [22]. Larger bandwidths can be made by the parallel coupling filters. The interdigital comb-line, quarter-wavelength resonators, and hairpin line are good candidates for narrowband designs.

Figure 9 depicts a simple structure of an open and short-circuited $\frac{\lambda}{4}$ stubs resonators and their equivalent circuits. When the quarter-wavelength resonator is open-circuited at its end (Figure 9(a)) low impedance is shown at its entering point, causing the attenuation of the RF signal entering this stub. Hence, the stub gives a band-stop response between the input and output ports. Herein, the stub is equivalent to a series capacitance C and inductance L. If the RF signal does not enter the stub which means a high impedance at this point, then a band-pass response can be produced, and the only way for that is to shorten the $\frac{\lambda}{4}$ resonator to the ground. The equivalent circuit of a quarter-wavelength short-circuited stub is given in Figure 9(b).

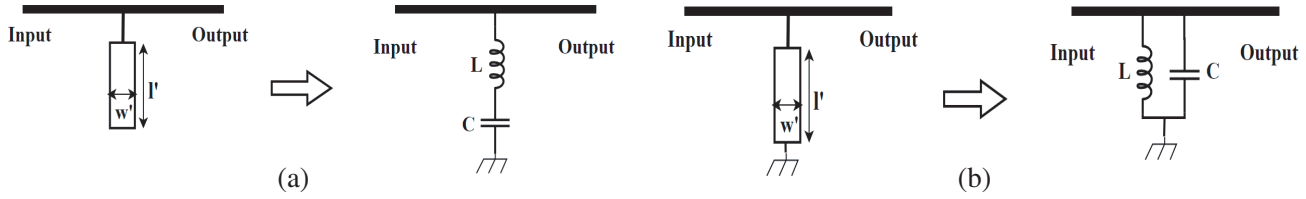

Figure 9. (a) Structure and equivalent circuit of Open-Circuited structure and (b) equivalent circuit of Short-Circuited, $\frac{\lambda}{4}$ stub resonator.

The values of the capacitance C and inductance L are calculated as in [23]. At first the effective dielectric constant ϵ_{eff} must be calculated from Equation (1) for $w'/t > 1$ [24]:

$$\epsilon_{eff} = \frac{\epsilon_r + 1}{2} + \left(\frac{\epsilon_r - 1}{2}\right)\left(\frac{1}{\sqrt{1 + 12\frac{t}{w'}}}\right) \tag{1}$$

where ϵ_r and t are the relative dielectric constant and the thickness of the substrate, and w' is the width of the stub.

For obtaining the characteristic impedance of the quarter-wavelength resonator we can use Equation (2) after calculating ϵ_{eff}.

$$Z_0 = \frac{120\Pi}{\sqrt{\epsilon_{eff}}\left(\frac{w'}{t} + 1.393 + 0.667\ln\left(\frac{w'}{t} + 1.444\right)\right)} \tag{2}$$

Then the length l' of the stub could be derived as a function of frequency f from Eq. (3). c presents the speed of light in the void.

$$l' = \frac{1.571}{\sqrt{\epsilon_{eff}}\left(\frac{2\Pi f}{c}\right)} \tag{3}$$

The inductance L and capacitance C are calculated according to the case: open-circuited or short-

circuited stub using the following:

$$\textit{Open-Circuited stub} \begin{cases} \omega_0 L = \dfrac{\Pi}{4} Z_0 \\ Z_0 = \dfrac{4}{\Pi}\sqrt{\dfrac{L}{C}} \end{cases} \tag{4}$$

$$\textit{Short-Circuited stub} \begin{cases} \omega_0 C = \dfrac{\Pi}{4}\dfrac{1}{Z_0} \\ Z_0 = \dfrac{4}{\Pi}\sqrt{\dfrac{L}{C}} \end{cases} \tag{5}$$

In this work, we used a narrowband band-pass filter of Semi-Square Semi-Circle shape derived from the quarter-wavelength resonators. The filter is constructed on the same substrate as the WB antenna (Rogers RO4725JXR). Figure 10 shows the proposed filter configuration. The proposed structure is of a coplanar waveguide type since it is composed of three conducting sections (two grounds and signal section) that are all on the same side of the substrate and are spaced by slots. We used a coplanar waveguide to implement the DGS filter because it has several benefits, including the fact that both the signal and ground plane are on the same surface. It can be easily integrated into existing RF integrated circuits with no need for via holes, and it is less sensitive to substrate thickness and dielectric constant. The band-pass filter can be derived from the same structure as the band-stop filter if the latter is shortened to the ground plane. Thus, two short-circuited stubs are calculated at quarter-wavelength of different resonant frequencies, and the band-pass response can be produced between those two frequencies as shown in Figure 11(b).

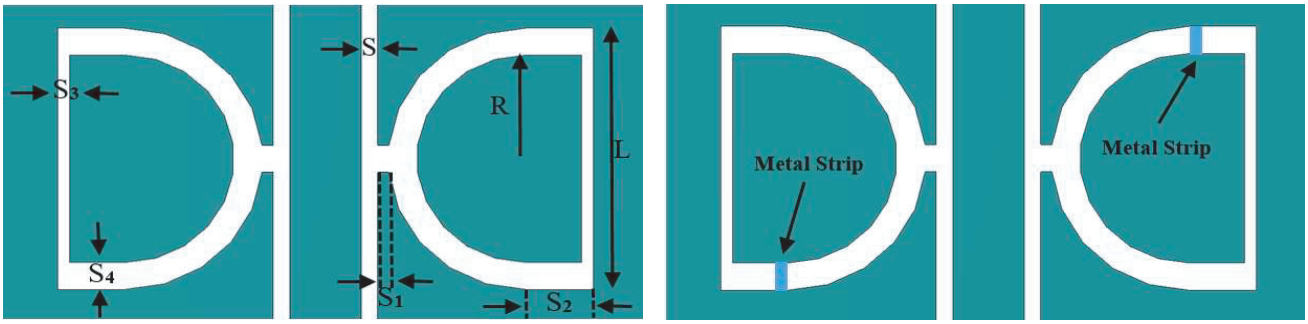

Figure 10. (a) Band-stop filter and (b) band-pass filter, configuration.

In the beginning, a band-stop filter has been designed. Figure 10(a) presents the proposed band-stop filter based on the $\frac{\lambda}{4}$ open-circuit stub. The filter rejects the incoming signals that have frequencies between 2.71 and 4.35 GHz, depicted by the insertion loss S_{21} in Figure 11(a). Moreover, the filter was etched in symmetry to the feed line so that the response sharpness could be effective. A distance S_1 of 0.27 mm was kept between the filter and the slotted line. The filter parameter values are presented in Table 1. In order to design the wanted filter, shown in Figure 11(b), small metal strips were mounted on the first band-stop filter for shortening the stubs to the ground plane and get the band-pass response as explained previously. The simulated S-parameters of the proposed filter, when the radius of the outer Semi-Circle is set to 5.8 mm, are illustrated in Figure 10. Hence, it can be seen from this figure that the response at 3.6 GHz is achieved with 15.77 dB return loss, where two poles are exhibited at different frequencies 3 and 4.82 GHz. Those poles were created with the help of metal strips when two short-circuited stubs of an effective length equal to 23.05 and 11.07 mm were cascaded respectively. As a result, a narrowband band-pass response was achieved with a fractional bandwidth of about 5% at the central frequency of 3.6 GHz. Consequently, the proposed filer proved its good frequency selectivity.

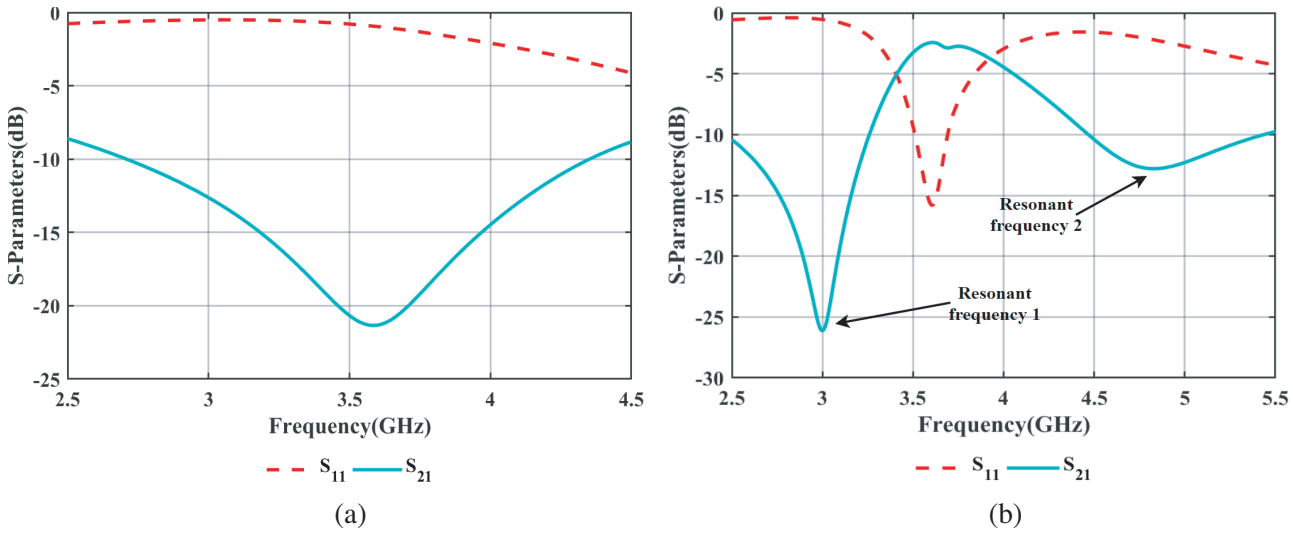

Figure 11. (a) Band-stop filter and (b) band-pass filter, simulated S-parameters.

Table 1. Parameters of the bandpass/bandstop filter in mm unit.

S_1	0.27	L	11.6
S_2	3	R	5.8
S_3	0.5	S	0.7
S_4	1.2		

4. FILTENNA SIMULATION AND MEASUREMENT RESULTS

Based on the previously proposed structures, the frequency tunable filtenna is established by incorporating the proposed Semi-Square Semi-Circle filter structure into the WB monopole antenna. The position of the filter depends on various criteria, as discussed in Section 2, so it should be placed in an area with a high concentration of the current density. It is noticed from Figure 8(b) that most of the current is situated at the slots near the feed-line and at the edges of the antenna, which means that those areas transmit the signal, so they are suitable for the filter. Since the targeted band is the European Sub-6 GHz between 3.4 and 3.8 GHz, the center frequency of the filter should be on this range in order to narrow the WB antenna bandwidth within the Sub-6 GHz spectrum. The filter-antenna is constructed based on the same substrate as the WB antenna and the filter.

Figure 12 shows the filter-antenna structure before adding the biasing network to the antenna and its corresponding simulated reflection coefficient in both CST and HFSS. These results were compared to the $|S_{11}|$ of the basic antenna to clearly see the effect of the proposed filter after its incorporation into the WB antenna ground plane. It can be observed from Figure 12(b) that the filtenna impedance bandwidth became narrow of nearly 12.56%, around the center frequency 3.66 GHz ranging from 3.43 to 3.89 GHz, while it was 25.38% before integration. The metal strips that were mounted at the filter slots as presented in Figure 12(a) will be replaced by varactor diodes to turn the antenna active, as proven in [25], which means placed in the same position. Thus, as shown the proposed filter is centered vertically on the ground plane to avoid its contact with the Subminiature Version A (SMA) connector and its coupling with the radiated element. The filter-antenna is well matched, at 3.62 GHz with 24.89 dB return loss in CST, and it is about 21 dB in HFSS. Although the filtenna results have a little deviation between the two simulators, they are in good agreement.

The surface current distribution is simulated at 2.5 and 3.6 GHz to validate the functionality of the

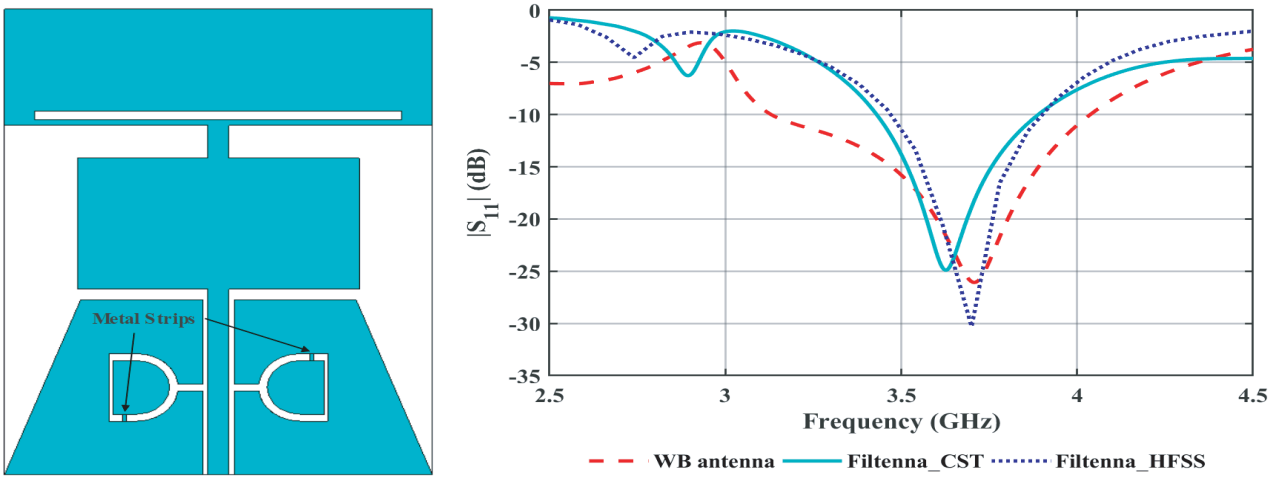

(a) (b)

Figure 12. (a) Filtenna configuration using metal strips and (b) return loss simulated results of the WB antenna compared to the filtenna with metal strips.

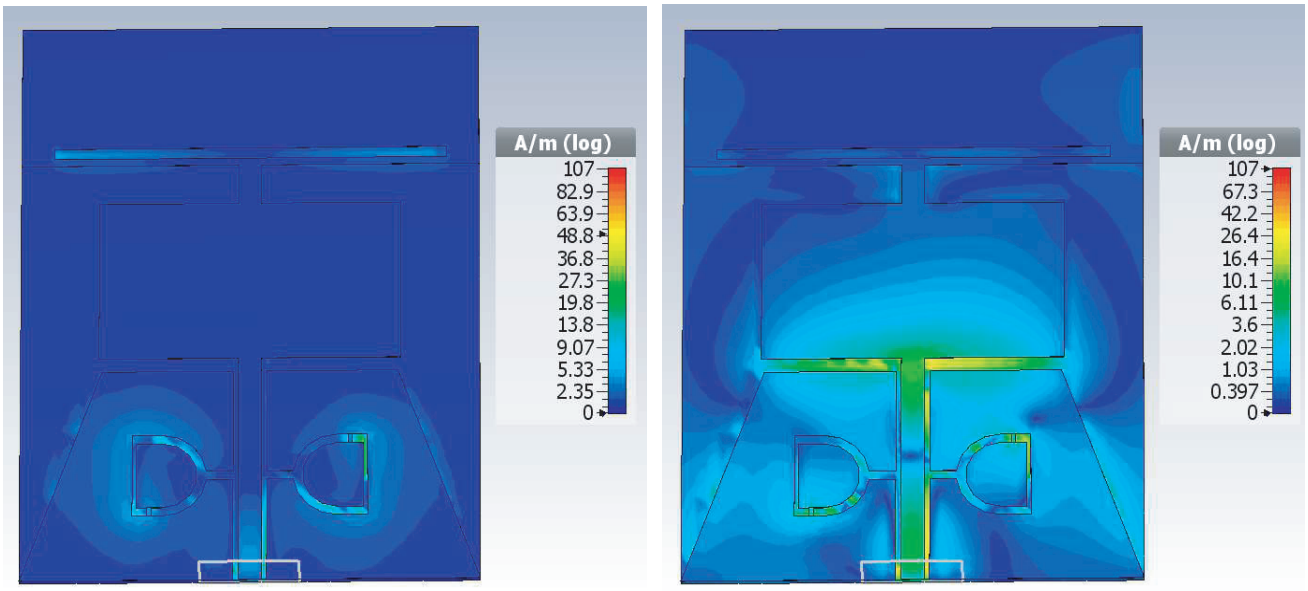

(a) (b)

Figure 13. Surface current distribution of the proposed filtenna at (a) 2.5 GHz and (b) 3.6 GHz.

filter, in out-of-band frequency and resonant frequency, respectively. It is demonstrated from Figure 13 that the filter reduces the current in the non-resonant frequency and helps to pass current to the patches in the working frequency.

Thanks to the advantages of variable capacitance diodes, we can realize an uncomplicated active antenna with frequency tunability operating in the Sub-6 GHz band. The varactor used has a model number BB659 from Infineon company, of Surface Mount Device (SMD) Mounting Style [26], and it simply helps to achieve a continuous frequency shift and specify the wanted operating frequency by changing its capacitance. Seen from this varactor datasheet, it exhibits an R parasitic series resistance of 0.6 Ω and an L_p parasitic series inductance of 0.6 nH. Figure 14 presents the equivalent circuit of this diode, where C_p is the controlling capacitance according to the chosen DC supply voltage. Changing the

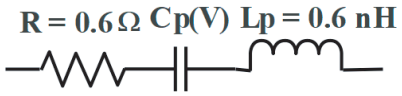

Figure 14. Equivalent circuit of varactor C_p = 2.4–40 pF.

diode's capacitance leads to the variation of current distribution, and this variation affects the electrical length of the DGS filter slots. On the other hand, the electrical length decreases by decreasing the capacitance which in return increases the resonant frequency and vice versa. In general, two varactors are used to tune the antenna resonant frequency, and they have a possible capacitance between 2.4 and 40 pF.

Controlling the varactors needs a DC voltage source, and in antennas or any other component the DC source should be separated from the RF signal, then a biasing network is necessary to polarize the varactor diodes. Accordingly, an RF shock is modeled by an SMD inductor of 39 nH in which the objective is to prevent the RF signal from passing to the DC source. Moreover, a horizontal slot that has 1.2 mm in width is used as a separator to isolate the ground plane from the transmitting part. A 27 pF capacitor is employed at the separator to ensure the RF signal continuity and decouple the DC signal. On the whole topology, the biasing circuits contain two varactors, four inductances, and four capacitors located symmetrically compared to the feed line as illustrated in Figure 15.

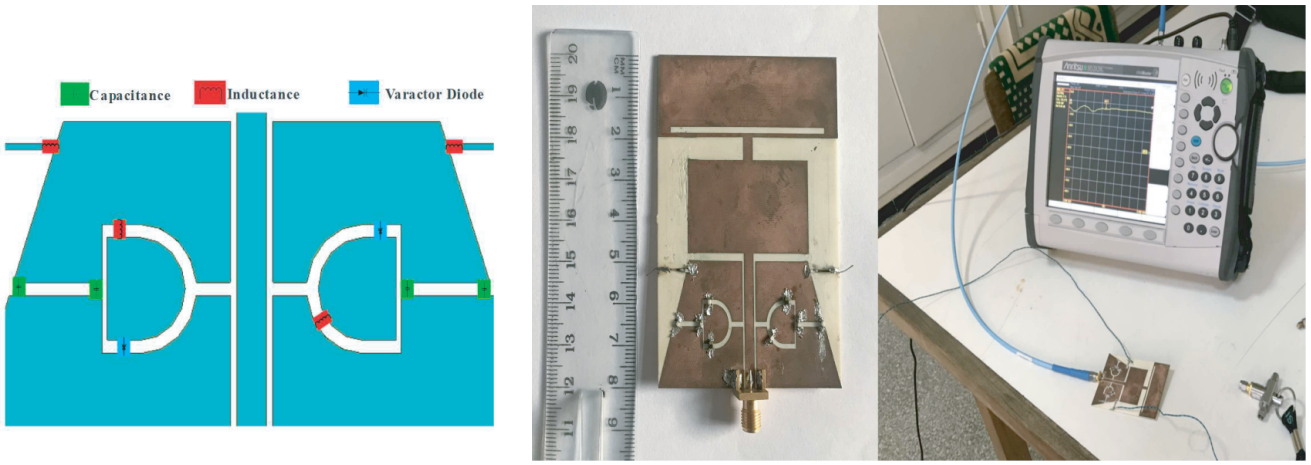

(a) (b)

Figure 15. (a) Biasing network and (b) photograph of fabrication/measurement, of the tunable filtenna.

By changing the reverse bias voltage applied to the diodes, the return loss in three cases was measured, then it was compared with the simulated results to demonstrate the tunable filtenna working capabilities. The junction capacitance of each varactor was set to 7.375 pF (10 V), 3.75 pF (22 V), and 2.4 pF (26 V). When the voltage is defined at 10 V, the filtenna operates at 3.4 GHz, and in the case to tune the resonant frequency to 3.6 GHz the DC power supply should be changed to 22 V, while the 3.8 GHz could be obtained when the voltage is set to 26 V. These tuning cases are within the desired band of Sub-6 GHz. In that way, the proposed filter-antenna showed its continuity of frequency shift within the frequency range 3.4–3.8 GHz that corresponds to voltage range 10–26 V. The corresponding results of the simulated/measured return loss, gain, and simulated radiation patterns are discussed in Figures 16, 17, and 18.

The S-parameters results are measured and compared with the simulated results which are displayed in Figure 16, for three cases within the Sub-6 GHz band (3.4, 3.6, and 3.8 GHz). It is found from this figure that the simulated return loss for the 10-dB impedance bandwidth using CST (HFSS) software is about 16.6 (13.4), 25.45 (18.6), and 20.71 (31.5) dB at the resonant frequencies 3.4, 3.6, and 3.8 GHz,

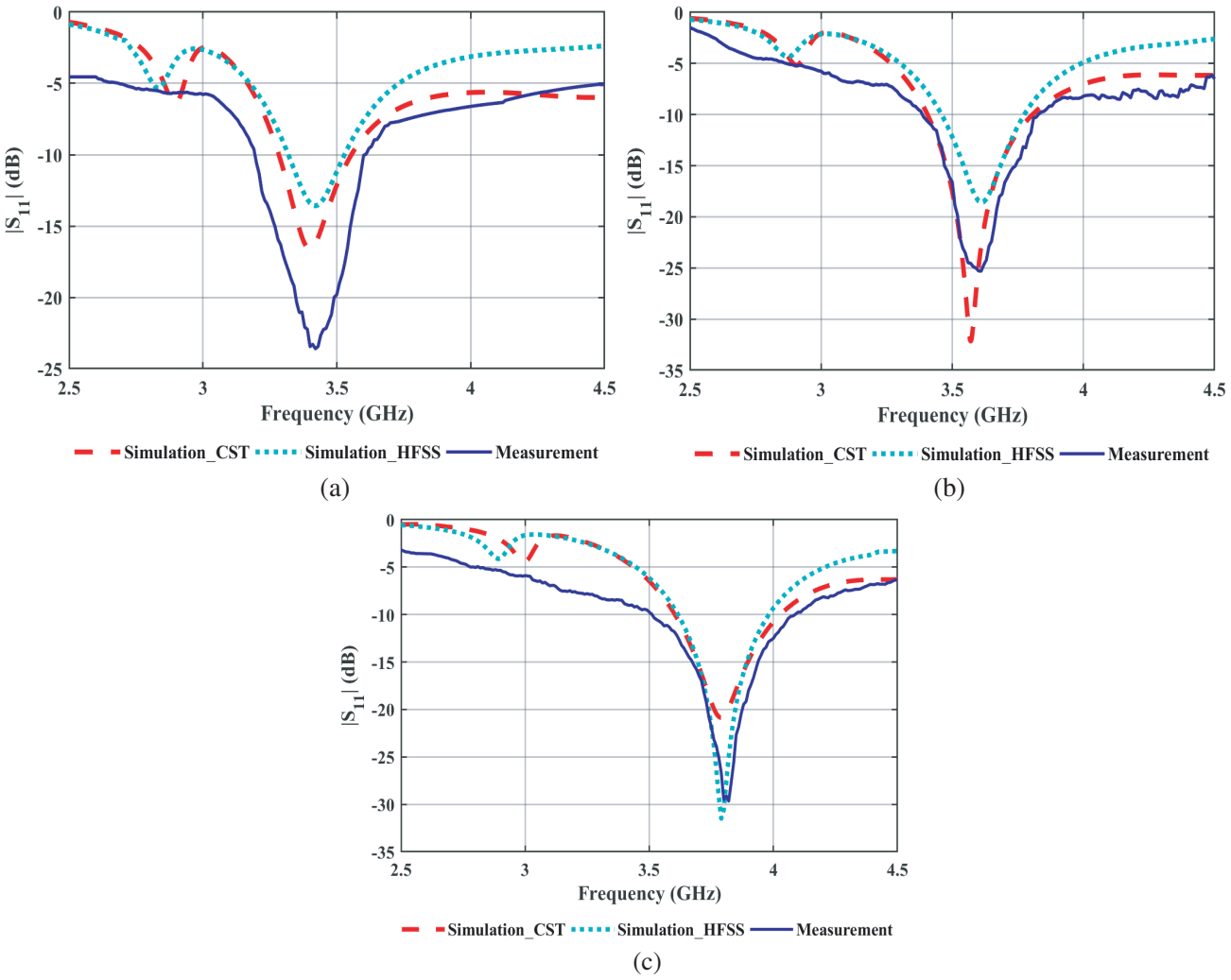

Figure 16. Simulation and measurement of filtenna return loss; (a) at 3.4 GHz (10 V), (b) at 3.6 GHz (22 V), and (c) 3.8 GHz (26 V).

respectively. On the other hand, measured results indicate that the proposed filtering-antenna gives a $|S11|$ of 23.45, 25.28, and 29.51 dB when the operating frequencies are respectively at 3.4, 3.6, and 3.8 GHz. In terms of bandwidth, the filtenna has a fractional bandwidth of 11.76% at 3.4 GHz, around 11.67% when the frequency is 3.6 GHz, and about 14.73% at 3.8 GHz.

Consequently, the filtering antenna provides a good frequency selectivity that changes automatically with the biasing voltage which gives the proposed antenna the flexible property. Simulated and measured results almost agree with each other. So, in addition to the reasons cited in Section 2, the small discrepancy between the results may be attributed to the non-availability of the anechoic chamber for measurement or the excitation method used, and the antenna was excited with a waveguide port in simulation, but in practice, the SMA connector was used instead.

Figure 17 gives the simulated and experimental realized gain values of the prototype developed versus frequency. The realized gain is investigated to guarantee that the variation of the resonant frequency does not influence the antenna characteristics. It can be observed from this figure that for measurements the maximum and minimum gains are obtained with 4.5 dBi and 3.9 dBi at 3.6 GHz and 3.4 GHz, respectively, and also the maximum gain is at 3.6 GHz with a value of 3.47 dBi, whereas the minimum value is 2.8 dBi at the frequency of 3.8 GHz for simulations. Therefore, these results have a neglected effect on the global functionality of the filter-antenna.

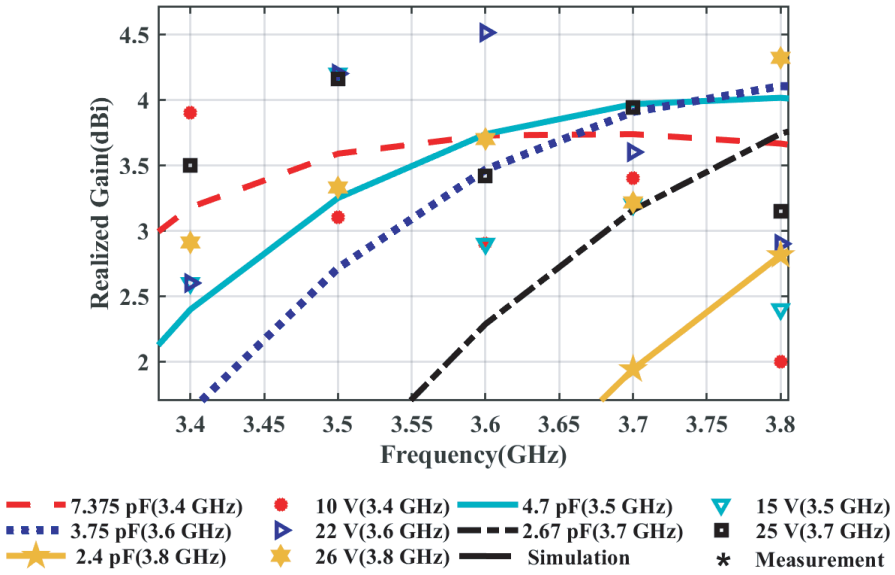

Figure 17. Realized gain of the proposed filtenna.

Here, the far-field performance was evaluated at three frequencies 3.4, 3.6, and 3.8 GHz for the two main planes $\Phi = 0°$ (i.e., corresponding to filtenna main radiation direction), and $\Phi = 90°$ (i.e., corresponding to the plane orthogonal to the main direction), as presented in Figure 18. It is possible to notice that the E-plane (angle $\Phi = 0°$) patterns are approximately omnidirectional, and in the H-plane ($\Phi = 90°$) the patterns reflect like a traditional monopole in the three studied cases. Hence, the filtenna polar patterns demonstrate that the given filtenna has a stable radiation behavior over the entire Sub-6 GHz band. Moreover, it has been shown that the proposed DGS Semi-Square Semi-Circle filter can keep a good impedance matching when shifting between resonant frequencies, and it can also provide excellent interference suppression and maintain some stable radiation properties. With those features, it is very vital for designing such an antenna to obtain CR communications for picocell base stations.

A comparison between the proposed work and previously reported antennas in the Sub-6 GHz is shown in Table 2, where FR refers to the working Frequency Range, and MG presents the maximum gain. TCT and NC are respectively the Tuning Components Type and the Number of Components used for tuning. It can be observed that unless [27] has a high gain of 8.2 dBi it is not tunable. Literatures [14–16] all tune their resonant frequency in the Sub-6 GHz band using different types of components, single-pole 4-throw(SP4T) switch, transceiver and varactors, but still, they all occupy a high space. Thus, our proposed structure covered the Sub-6 GHz band using two varactor diodes in lower dimensions with higher gain than the cited papers. Herein, the varactor diode has been chosen as a tuning component since it has a high-temperature sensitivity, low cost, and it is widely commercially available compared to the other components.

Table 2. Comparison between the proposed antenna and related works.

Ref.	FR (GHz)	MG (dBi)	TCT	NC	Antenna size (mm^3)	Yes
[14]	2.5–3.6	1.7	SP4T	1	$60 \times 100 \times 1$	Yes
[15]	1.7–6	Not given	Transceiver	1	$136 \times 68 \times 6$	Yes
[16]	3.49–3.87	3	Varactor	2	$80 \times 80 \times 2.4$	Yes
[27]	3.17–3.77	8.2	—	—	$80 \times 80 \times 5.813$	No
Pro. work	3.4–3.8	4.5	Varactor	2	$60 \times 80 \times 0.77$	Yes

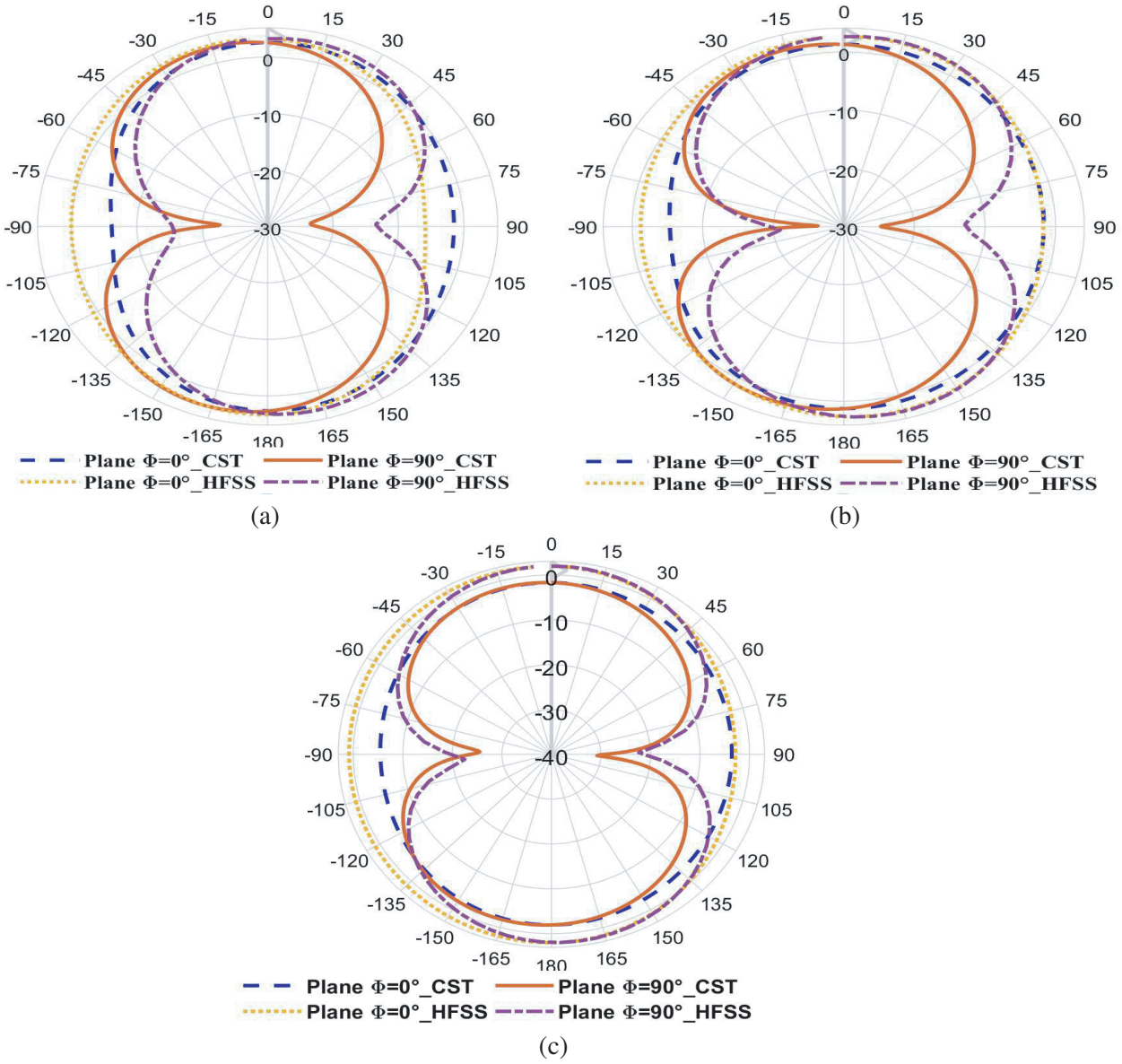

Figure 18. Simulated radiation patterns for plane $\Phi = 0°$ and $\Phi = 90°$ of the proposed filtenna at (a) 3.4 GHz, (b) 3.6 GHz and (c) 3.8 GHz.

5. CONCLUSION

Based on a WB monopole antenna with a defected ground structure, containing a Semi-Square Semi-Circle band-pass filter, a frequency tunable filtenna for CR picocell base stations has been proposed. The continuous shift of operating frequency has been achieved using two varactor diodes located at the filter slots and controlled by changing the reverse bias voltage. In order to narrow the WB antenna bandwidth for communication task, the filter has been incorporated into its ground plane. The simulated (measured) results demonstrated that the WB antenna can operate between 3.13 and 4.04 GHz (3.15 and 4.19 GHz) corresponding to 25.38% (28.33%) fractional bandwidth. Therefore, the filtenna operating frequency goes from 3.4 to 3.8 GHz when the DC voltage goes from 10 to 26 V. Simulated and measured results have shown a reflection coefficient at three frequencies 3.4, 3.6, and 3.8 GHz, and its values are equal to 16.6 (23.45), 25.45 (25.28), and 20.71 (29.51) dB, respectively. The maximum realized gain

of the filtenna is about 3.47 dBi in simulations and 4.5 dBi in measurements. Moreover, the radiation patterns results were stable while changing the bias voltage and proved the omni-directionality of the filter-antenna beams. Consequently, the proposed filtenna can be found useful in many picocell base stations more specifically in the Sub-6 GHz band.

ACKNOWLEDGMENT

The authors of this paper would like to express their deepest thanks to the Department of Engineering and Communications at the University of Cantabria, Santander, Spain, and especially Professor Angel Mediavilla for his help concerning simulation software.

REFERENCES

1. "Wired vs. Wireless Technologies for Communication Networks in Utility Markets," https://www.utilityproducts.com/test-measurement/article/16002788/wired-vs-wireless-technologies-for-communication-networks-in-utility-markets, January 7, 2022.
2. "Vodafone and Samsung strategic partnership to launch Smart Home services," https://www.vodafone.com/news-and-media/vodafone-group-releases/news/vodafone-and-samsung-strategic-partership, January 7, 2022.
3. "Global update on spectrum for 4G and 5G," https://www.qualcomm.com/media/documents/files/spectrum-for-4g-and-5g.pdf, December 2020.
4. Dudzinsky, Jr., S. J., "Atmospheric effect on terrestrial millimeter-wave communication," https://www.rand.org., March 1974.
5. Kusaladharma, S. and C. Tellambura, "An overview of cognitive radio networks," *Wiley Encycl. Electr. Electron. Eng.*, August 2017.
6. Kingsly, S., D. Thangarasu, M. Kanagasabai, M. Gulam Nabi Alsath, R. R. Thipparaju, S. K. Palaniswamy, and P. Sambandam, "Multiband reconfigurable filtering monopole antenna for cognitive radio applications," *IEEE Antennas Wirel. Propag. Lett.*, Vol. 17, No. 8, 1416–1420, 2018.
7. Tang, M. C., Z. Wen, H. Wang, M. Li, and R. W. Ziolkowski, "Compact, Frequency-reconfigurable filtenna with sharply defined wideband and continuously tunable narrowband states," *IEEE Trans. Antennas Propag.*, Vol. 65, No. 10, 5026–5034, 2017.
8. Mishra, S. R. and S. Kochuthundil Lalitha, "Filtennas for wireless application: A review," *Int. J. RF Microw. Comput. Aided Eng.*, Vol. 29, No. 10, 1–28, 2019.
9. Nella, A. and A. S. Gandhi, "A five-port integrated UWB and narrowband antennas system design for CR applications," *IEEE Trans. Antennas Propag.*, Vol. 66, No. 4, 1669–1676, 2018.
10. Nachouane, H., A. Najid, A. Tribak, and F. Riouch, "Dual port antenna combining sensing and communication tasks for cognitive radio," *International Journal of Electronics and Telecommunications*, Vol. 62, No. 2, 121–127, 2016.
11. Srikar, D. and S. Anuradha, "A compact 3 port integrated wide band sensing antenna and narrow band antennas for cognitive radio applications," *2019 PhotonIcs & Electromagnetics Research Symposium — Spring (PIERS — Spring)*, Rome, Italy, June 17–20, 2019.
12. Ramadan, A. H., J. Costantine, M. Al-Husseini, K. Y. Kabalan, Y. Tawk, and C. G. Christodoulou, "Tunable filter-antennas for cognitive radio applications," *Progress In Electromagnetics Research B*, Vol. 57, 253–265, 2014.
13. Atallah, H. A., A. B. Abdel-Rahman, K. Yoshitomi, and R. K. Pokharel, "Compact frequency reconfigurable filtennas using varactor loaded T-shaped and H-shaped resonators for cognitive radio applications," *IET Microwaves, Antennas Propag.*, Vol. 10, No. 9, 991–1001, 2016.
14. Lee, W. W. and B. Jang, "A tunable MIMO antenna with dual-port structure for mobile phones," *IEEE Access*, Vol. 7, 34113–34120, 2019.

15. Hannula, J. M., T. O. Saarinen, A. Lehtovuori, J. Holopainen, and V. Viikari, "Tunable eight-element MIMO antenna based on the antenna cluster concept," *IET Microwaves, Antennas Propag.*, Vol. 13, No. 7, 959–965, 2019.
16. Ikeda, T., S. Saito, and Y. Kimura, "A frequency-tunable varactor-loaded single-layer ring microstrip antennas fed by an L-probe with a reduced bias circuit," *2017 International Symposium on Antennas and Propagation (ISAP)*, Thailand, October 30–November 2, 2017.
17. Fischer, B. E., I. J. Lahaie, M. D. Huang, M. H. A. J. Herben, A. C. F. Reniers, and P. F. M. Smulders, "Measurements corner: Causes of discrepancies between measurements and em simulations of millimeter-wave antennas," *IEEE Antennas Propag. Mag.*, Vol. 55, No. 6, 139–149, 2013.
18. Chen, C. J., "Design of parallel-coupled dual-mode resonator bandpass filters," *IEEE Trans. Components, Packag. Manuf. Technol.*, Vol. 6, No. 10, 1542–1548, 2016.
19. Liu, Q., D. F. Zhou, D. W. Zhang, D. L. Lu, and Y. Zhang, "Dual-mode microstrip patch bandpass filters with generalized frequency responses," *IEEE Access*, Vol. 7, 163537–163546, 2019.
20. Shome, P. P. and T. Khan, "A quintuple mode resonator based bandpass filter for ultra-wideband applications," *Microsyst. Technol.*, Vol. 26, 2295–2304, 2020.
21. Lin, S. C., P. H. Deng, Y. S. Lin, C. H. Wang, and C. H. Chen, "Wide-stopband microstrip bandpass filters using dissimilar quarter-wavelength stepped-impedance resonators," *IEEE Trans. Microw. Theory Tech.*, Vol. 54, No. 3, 1011–1018, 2006.
22. Sekiya, N. and S. Sugiyama, "HTS dual-band bandpass filters using stub-loaded hair-pin resonators for mobile communication systems," *Phys. C Supercond. and Its Appl.*, Vol. 504, 88–92, 2014.
23. Pozar, D. M., *Microwave Engineering*, John Wiley & Sons, 2011.
24. Balanis, C. A., *Advanced Engineering Electromagnetic*, John Wiley & Sons, 1999.
25. Zhang, Z., F. Zhao, and A. Wu, "A tunable open ring coupling structure and its application in fully tunable bandpass filter," *Int. J. Microw. Wirel. Technol.*, Vol. 11, No. 8, 782–786, 2019.
26. Varactor Diode BB659, Data Sheet, Semiconductor and System Solutions-Infineon Technologies. https://www.infineon.com/, January 6, 2022.
27. Wen, L. H., S. Gao, Q. Luo, Q. Yang, W. Hu, and Y. Yin, "A low-cost differentially driven dual-polarized patch antenna by using open-loop resonators," *IEEE Trans. Antennas Propag.*, Vol. 67, No. 4, 2745–2750, 2019.